npj | climate and atmospheric science

Article

Published in partnership with CECCR at King Abdulaziz University

https://doi.org/10.1038/s41612-026-01422-8

Real-time monitoring of H_2S emissions from the Pisciarelli fumarole at Phlegraean Fields with a Quartz-Enhanced Photoacoustic sensor

Check for updates

Arianna Elefante[1], Mariagrazia Olivieri[2], Vincenzo Luigi Spagnolo[2,3], Angelo Sampaolo[2,3], Silvia Massaro[4], Roberto Sulpizio[4,5], Pierfrancesco Dellino[4], Francesco Rufino[6], Stefano Caliro[6], Antonio Costa[5] & Pietro Patimisco[3,7] ✉

The persistent unrest at Campi Flegrei highlights the importance of accurate and continuous surveillance of volcanic gas emissions to support scientific interpretation and civil protection efforts. Suitable sensors capable of fast, real-time tracking of trace gas components within CO_2-H_2O -dominated fumarolic plumes are still missing. In this work, a compact Quartz-Enhanced Photoacoustic Spectroscopy (QEPAS) sensor was used for real-time and in situ detection of the hydrogen sulfide (H_2S) emitted from the Pisciarelli fumarolic field at the Campi Flegrei caldera. The 1 s response time of the sensor allows the capture of the fast emission dynamics of the plume and accurate reconstruction of H_2S emission peaks up to 60 part-per-million (ppm). By combining the QEPAS measurements with a commercial non-dispersive infrared spectroscopy CO_2 sensor, a characteristic CO_2/H_2S ratio of 208 ± 4 was estimated for the Pisciarelli fumarolic field.

Volcano surveillance is a central pillar in volcanology, aimed at identifying and interpreting the reawakening signs of dormant volcanoes to mitigate hazards while helping in reducing false alarms. The complexity of eruptive dynamics requires a multi-parametric monitoring system based on networks of heterogeneous sensors, which are capable to track the most recurrent indicators of unrest, such as variations of the degassing processes, ground deformation and increase in seismic activity[1]. The reliable acquisition and analysis of these data provide the primary tool to investigate and understand the mechanisms driving volcanic unrest.

The ongoing phase of unrest at the Campi Flegrei caldera (CFc) in Italy represents a newsworthy case study. According to conceptual geochemical models, the CFc hosts an active hydrothermal system at a depth of ~3 km, characterized by a continuous release into the atmosphere of gas plumes formed by the interaction between boiling meteoric waters and hot gases ascending from a magmatic chamber estimated at a depth of ~8 km[2,3]. This gas plume continuously feeds fumaroles, most notably at Solfatara crater and Pisciarelli vent (Fig. 1a).

After the last eruption occurred in 1538 (Monte Nuovo) and the subsequent quiescent period, the CFc has experienced recurrent unrest since 1950, characterized by four bradyseism cycles with the last, which started in 2005, currently going on[4]. This sustained activity has driven intense scientific attention, resulting in high number of scientific papers over the past decade, mainly focused on the analysis and interpretation of the ground deformation and seismicity data in an effort to elucidate the underlying driving processes, e.g., refs. 5,6. Both ground deformation and seismicity have been interpreted as the elastic/brittle response of the shallow crust to the pressure exerted at the base of the hydrothermal system by escalating magmatic fluid transport.

Besides geodetic and seismic observations, the analysis of plume composition provides an essential piece to the puzzle for understanding volcanic systems. Monitoring gas emissions released into the atmosphere from both magmatic and hydrothermal systems can provide a description of magma degassing processes occurring at different depths within the mantle, the crust, and the hydrosphere[7,8]. The chemical and isotopic composition of the plume, together with abundances, fluxes and their temporal variability,

[1]National Research Council, Institute for Photonics and Nanotechnologies, Bari, Italy. [2]Polytechnic University of Bari, Bari, Italy. [3]PolySense Innovations srl, Bari, Italy. [4]Department of Earth and Geoenvironmental Sciences, University of Bari Aldo Moro, Bari, Italy. [5]National Institute of Geophysics and Vulcanology, Bologna, Italy. [6]National Institute of Geophysics and Vulcanology, Osservatorio Vesuviano, Napoli, Italy. [7]Department of Physics, University of Bari Aldo Moro, Bari, Italy. ✉e-mail: pietro.patimisco@uniba.it

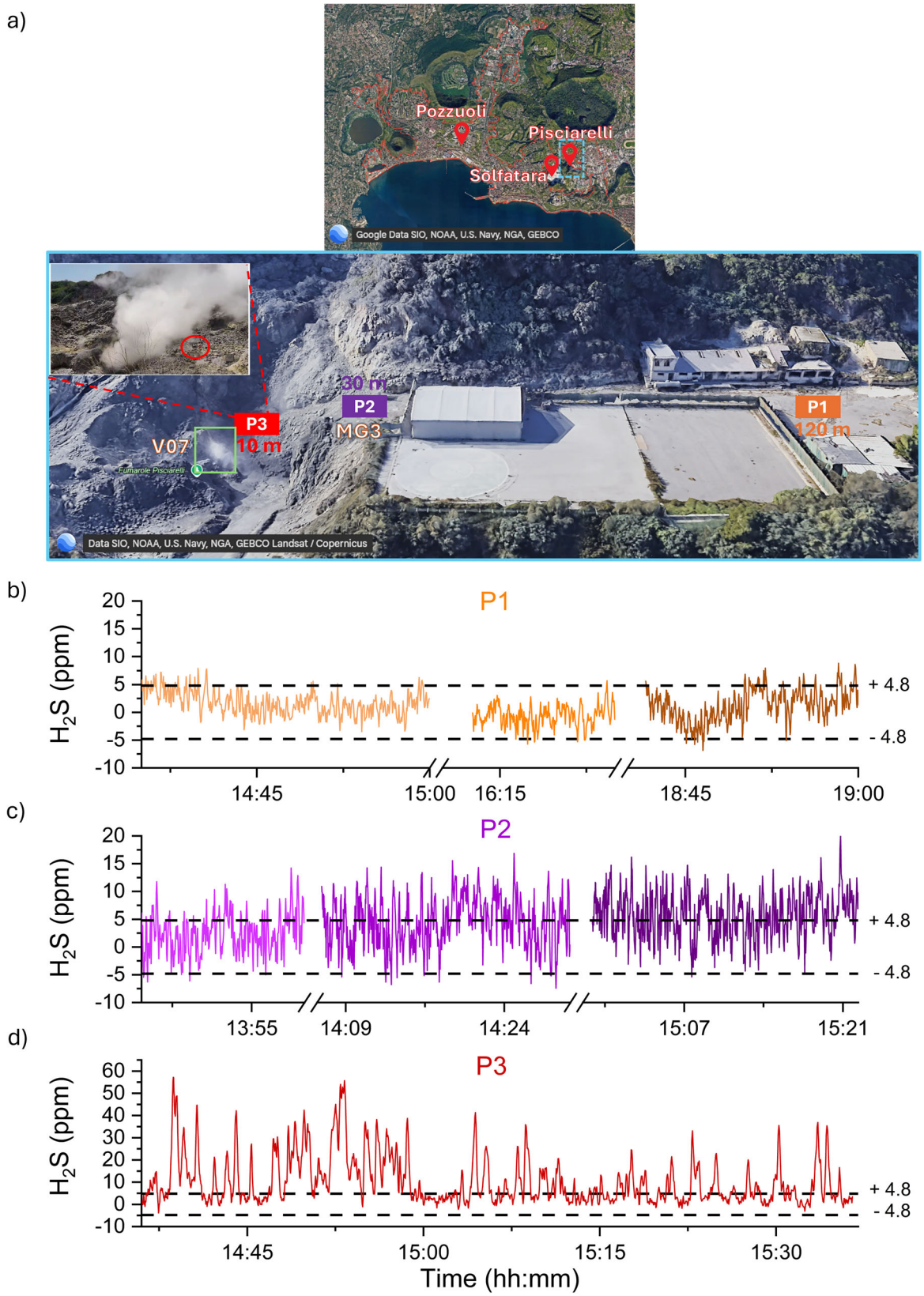

Fig. 1 | Location of the Pisciarelli fumarolic field measurement site and H_2S concentrations at different distances from the emission source. a Google Earth view of the Pisciarelli fumarolic field at the CFc showing the location of the investigated plume and the measurement positions[45]. H_2S time series measured using the QEPAS sensor at distance of 120 m (P1) (**b**), 30 m (P2) (**c**) and 10 m (P3) (**d**) from the fumarolic plume.

Table 1 | Typical techniques implemented for geochemical monitoring of volcanoes with their temporal resolution

Technique	Sampling	Target molecules	Response Time	Ref
Gas Chromatography- Mass Spectroscopy Wet chemical	Off-line	N_2, Ar, O_2, H_2, CO, COS, hydrocarbons, noble gases, CO_2, SO_2, H_2S, HCl, HF	Hours	12
UV spectrometer	On-line	SO_2	~mins	14
UV camera	On-line	SO_2	1 s	16
Open-path FTIR spectrometer	On-line	O_2, H_2O, SO_2, HCl, and HF	~mins	17
Electrochemical	On-line	H_2S, SO_2, H_2	30-60 s	24,42

provides valuable information into the state of activity of a volcano[7,9]. Volcanic plumes are complex gaseous mixtures composed in percentage by H_2O and CO_2, with minor constituents present at trace concentrations that depend on the nature and depth of the source. Magmatic systems are typically enriched in SO_2, HCl, HF, and CO, which are usually absent in hydrothermal systems, such as at CFc, due to the interaction with aquifers, resulting in emissions dominated by H_2S and CH_4. In particular, the sulfur degassing and its temporal evolution are widely recognized as geochemical indicators of a transition from hydrothermal to magmatic-dominated regimes[10] and as tracers of escalating volcanic unrest[11]. Moreover, the sulfur isotopic analysis ($\delta^{34}S$) provides information on sulfur provenance, allowing discrimination among magmatic source, meteoric fluids, sedimentary rocks or associated fluids, seawater, or other potential sources[12].

Identifying suitable and reliable gas sensing techniques deployable in harsh volcanic environments remains a major challenge. Table 1 reports typical sensor systems applied worldwide to characterize the chemical composition of volcanic plumes, underlining in particular their different temporal resolution. Historically, the most widely adopted approach has relied on gas sampling using evacuated glass flasks and subsequent analysis in the laboratory with gas chromatography-mass spectrometry and wet-chemical techniques. Despite its broad applicability, this sampling-based approach is susceptible to sample alteration caused by condensation, re-evaporation, and chemical reactions[12] during collection, storing and handling. Most importantly, the off-line laboratory analysis is time consuming, requiring hours for one sample and it does not allow real-time measurements or direct assessment of the gas flow from the fumarolic vents. To overcome these limitations, near real-time and in-situ measurements have been pursued using spectroscopic techniques and electrochemical (EC) sensors. Correlation spectrometers[13,14], ultraviolet (UV) fiber-optic differential optical absorption spectrometers[15] and UV cameras[16] have been implemented for SO_2 measurements, exploiting its strong UV absorption. In particular, the UV cameras offer a temporal resolution of 1 Hz which could allow to capture transient volcanic degassing phenomena which are unresolved using traditional scanning spectrometers with sampling rates of few minutes. Nevertheless, their applicability is largely restricted to high temperature fumaroles analysis (T >400 °C) whose emissions are SO_2-dominated, differently from the CFc low-temperature fumaroles. Open-path Fourier Infrared Spectroscopy, combined with atmospheric transfer models, enables the simultaneous detection of multiple species, as CO_2, H_2O, SO_2, HCl, and HF[17]. Among compact, field-deployable solutions, the MultiGAS sensor system [18] provides a low-cost, low-power and compact solution for in-situ continuous monitoring of volcanic gases. It combines non-dispersive infrared (NDIR) sensor for H_2O and CO_2 detection with three EC sensors for reactive gases: SO_2, H_2S and H_2. EC sensors detect gases by oxidation-reduction reactions triggered by the interaction of the target molecules with an electrochemical substrate, generating an electrical signal proportional to the analyte concentration. Due to their relatively low cost (hundreds of euros), low power consumption (few mW), compactness, and sub-ppm sensitivity, EC sensors are well suited for large-scale deployments and provide high spatial coverage in volcanic monitoring networks. However, several well-known limitations must be considered when operating EC sensors outdoor and, in particular, in volcanic environments. EC sensors can exhibit signal drift due to temperature and humidity variations, as well as performance degradation over time, requiring frequent recalibrations. Moreover, they suffer from chemical cross-sensitivities, which limit their selectivity when targeting a specific analyte in a complex and dynamically changing gas matrix. Most importantly, EC sensors are characterized by slow response and recovery times (30 - 60 s), precluding their capability to capture fast variations in the gas concentration[18]. Considering these aspects, EC sensors are particularly suitable for monitoring networks aimed at safety control, regulatory compliance, and long-term trend analysis. However, their limited temporal resolution and selectivity may reduce data reliability when monitoring rapidly evolving gas compositions in highly dynamic volcanic plumes.

Among the different techniques, the chemical composition of the fumarolic gases at the CFc has been systematically measured since 1985 through monthly sampling followed by off-line laboratory analysis, retrieving the concentration of H_2O, CO_2, H_2S, Ar, N_2, H_2, CH_4, and CO. The resulting long-term compositional datasets have been extensively used to investigate correlations between fumarolic chemical composition and geophysical and seismic observations[2,5,19], supporting the development and validation of geochemical models of the CFc on the decades-long time scale. These models, based on hydrothermal gas equilibria and numerical simulations of the magmatic degassing, successfully reproduce the observed compositional trends, evaluate the feasibility of the processes hypothesized and estimate the temperature-pressure conditions of the system, enabling projections of its future evolution[2,20]. Most existing geochemical models primarily rely on the H_2O–CO_2–N_2–He–Ar dataset, as documented in several studies of the CFc[21,22]. In contrast, fewer investigations have incorporated direct measurements of the CO_2 fluxes from fumarolic vents, typically obtained using Tunable Diode Laser Spectroscopy[23], or the MultiGAS sensor[24].

More recently, increased attention has been given to the hydrogen sulfide (H_2S) content within the 40-year fumarolic gas dataset. An unprecedented increase in the H_2S concentrations, along with a decrease in the $\delta^{34}S$ value of H_2S has been happening since 2018, and has been interpreted as decompression-driven degassing of mafic magma at depths ≥6 km, combined with partial sulfur remobilization from hydrothermal minerals[11].

Compared to CO_2 monitoring, the detection of trace gases like H_2S is more critical. The current monitoring strategy adopted by the Istituto Nazionale di Geofisica e Vulcanologia (INGV) is based on monthly fumarolic gas sampling followed by laboratory analysis, complemented by daily (hourly) in situ measurements using the MultiGAS station. Specifically, the amperometric AlphaSense H2S-B4 EC sensor embedded in the MultiGas station at Campi Flegrei shows a response time of 60 s, as well as cross-sensitivities to several gas species, including CO, NO, NO_2, SO_2 and H_2, as well as temperature-dependent background and sensitivity in the 20–50 °C temperature range. The availability of a sensor capable of in-situ and real-time detection of H_2S traces with high selectivity, sensitivity and fast response time would overcome many of the limitations of existing approaches. In particular, high temporal resolution is essential to follow the H_2S chemical kinetics and accurately capture transient emission peaks, which are likely to be missed by slow-response sensors, leading to systematic underestimation of H_2S concentration and flux[25]. It is well established that H_2S dynamics strongly depend on atmospheric stability and meteorological factors, particularly precipitation, air humidity, temperature, and wind

regime[26,27]. Observational studies showed that short-lived but intense pollution episodes are associated with stable and inversion-prone conditions[28]. Additionally, H_2S is commonly assumed to be rapidly oxidized to SO_2 via reactions with OH radicals[29], but both observational and experimental evidence indicate that this conversion may be incomplete or delayed depending on the local environmental conditions[30].

As a result, sulfur atmospheric chemistry remains complex and poorly constrained for geothermally emitted H_2S, with reported oxidation rates varying widely[29]. More detailed kinetic investigations and appropriate calibration of numerical dispersion models that adequately account for atmospheric stability effects are required to properly evaluate H_2S chemical processing in volcanic plumes. At the same time, the high temporal-resolution measurements of H_2S can serve broader environmental and climate-related studies helping at investigating the influence of hydrothermal and fumarolic emissions on local air quality, atmospheric chemistry, and the natural sulfur cycling[26,27]. In this context, the development of fast-response and precise techniques for H_2S detection is essential to better constrain short-term variability in gas emissions, improve the quantification of natural sulfur fluxes from geothermal and hydrothermal areas, and support atmospheric dispersion and chemical transformation studies.

In this work, we present the implementation of a compact Quartz-Enhanced Photoacoustic Spectroscopy (QEPAS) sensor as a potential solution for on-site detection of H_2S in volcanic areas with high temporal resolution. The QEPAS technique has demonstrated to provide high selectivity and sensitivity for the detection of several gas species at the ppm-ppb concentration levels[31], together with fast response times on the order of seconds or sub-seconds, enabling real-time tracking of rapid variations in gas emission in the environment[32]. The QEPAS sensor was combined with a commercial GasLab®Pro analyzer to simultaneously monitor CO_2 and H_2O in the volcanic plume. The resulting multi-sensor platform was first tested and calibrated under controlled laboratory conditions and subsequently deployed at the Pisciarelli fumarolic field for real-time, in-situ measurements of plume composition.

Results

Real-time, in-situ measurements of the volcanic plume composition were carried out at the Pisciarelli fumarolic field during May 28-29, 2025. Multiple gas species were tracked simultaneously, including H_2O, CO_2 and H_2S using a sensing platform composed of a GasLab®Pro analyzer and a QEPAS sensor. The most abundant components, CO_2 and H_2O, present at percent-level concentrations, were monitored using the GasLab®Pro analyzer based on a NDIR sensor and an electronic hygrometer. Highly sensitive and selective detection of trace-level H_2S was performed using a QEPAS sensor. Several measurement campaigns were conducted to characterize the spatial distribution of the H_2S emissions, investigate their temporal variability, and determine the H_2S/CO_2 geochemical indicator.

H_2S Spatial distribution

The first investigation focused on evaluating H_2S concentrations in ambient air at different distances from the fumarolic source. Fig. 1a) shows the location of the investigated plume (green box) and the three measurement positions where the sensing platform was deployed, corresponding to distances of 120 m (P1), 30 m (P2) and 10 m (P3) from the source. The corresponding H_2S QEPAS time series measured at each point are reported in (Fig. 1b–d). The black dashed line indicates the 3σ minimum detection limit (MDL) of the QEPAS sensor, corresponding to 4.8 ppm, as described in the Methods Section.

At the greatest distance (P1), the H_2S signal exhibited only fluctuations within the MDL threshold, comparable to the noise level acquired during laboratory tests (see Methods Section). If present, ambient H_2S concentrations at this location were therefore below 4.8 ppm (Fig. 1b). At the intermediate distance (P2), signal variations exceeding the MDL threshold were detected (Fig. 1c). At the closest distance (P3), the sensing platform was directly invested by the plume, depending on the wind direction, and pronounced H_2S peaks up to 60 ppm were detected, with a mean concentration value of 11.5 ppm over the 60-minute measurement interval shown in Fig. 1d).

H_2S temporal variation

To investigate the temporal variability of H_2S emissions, the sensing platform was fixed at position P3 and measurements were conducted on two consecutive days. Fig. 2 shows the H_2S time series acquired on 28 May (a) and 29 May (b), 2025. The QEPAS sensor was operated with an integration time of 1 s and an acquisition time of 2 s, providing sufficient temporal resolution to capture the fast emission dynamics of the plume. This allowed accurate reconstruction of transient H_2S emission peaks without loss of information, as highlighted in the enlarged view in Fig. 2c). Such high temporal resolution represents a key advantage over electrochemical sensors, whose slow response and recovery time (on the order of tens of seconds) preclude reliable tracking of emission dynamics on sub-minutes timescales[33].

During the measurements, H_2S detection was periodically interrupted to verify the correct operation of the QEPAS sensor through two

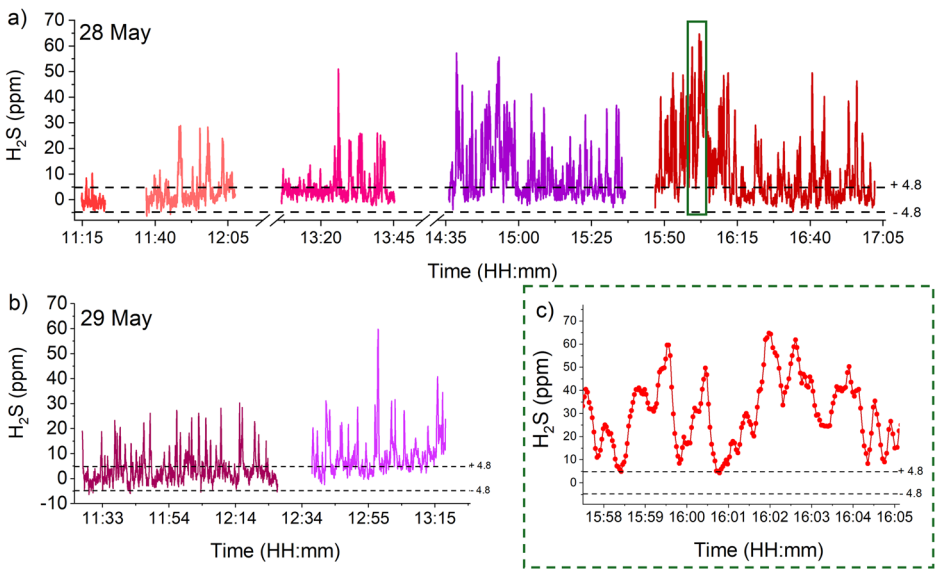

Fig. 2 | Temporal variation of the H_2S concentration over two days of measurements. H_2S QEPAS signals acquired on 28 May (**a**) and 29 May (**b**) at position P3. Different colors are used to indicate the restarting of the measurement after periodic interruptions for control procedures; **c** Enlarged view of the H_2S QEPAS on a timescale of 8 min.

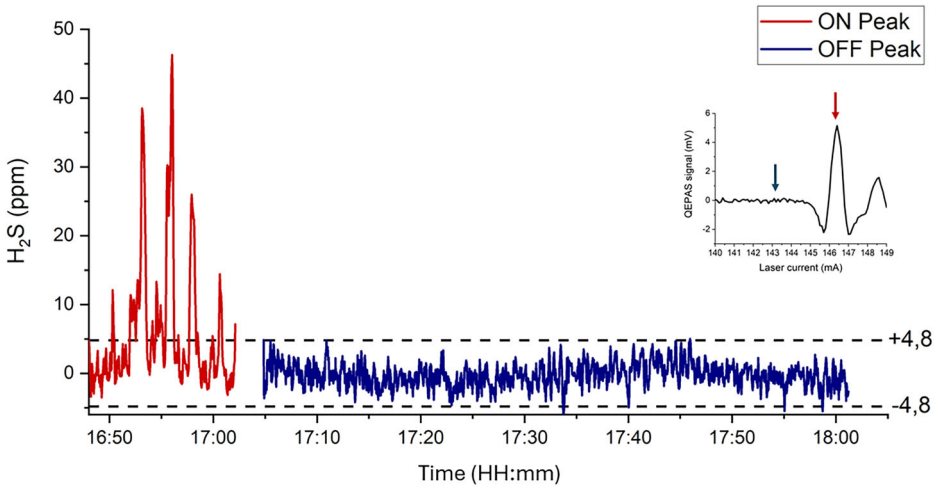

Fig. 3 | QEPAS peak signal acquired at position P3 with the laser current set to I = 146.4 mA, corresponding to the H_2S absorption line at 3792.9 cm-1 (red trace) and to I = 143 mA, corresponding to a wavelength at which no H_2S absorption lines are present (blue trace). Inset: QEPAS spectral scan of the H_2S acquired in the laboratory, with arrows indicating the peak current I = 146.4 mA (red arrow) and the off-peak current I = 143 mA (blue arrow).

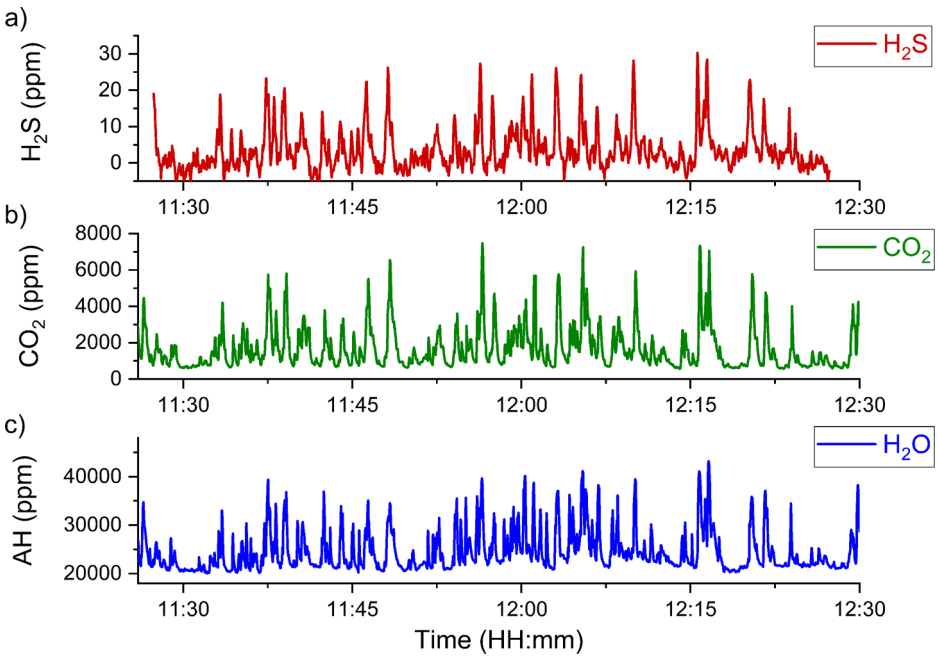

Fig. 4 | Simultaneous detection of H_2S, H_2O and CO_2. Concentration time series of **a** the H_2S signal detected using the QEPAS sensor; the CO_2 (**b**) and the H_2O (**c**) signals detected using the GasLab®Pro sensor.

complementary control procedures. First, the electrical characterization of the acoustic detection module (ADM) of the QEPAS sensor was performed to verify the stability of the resonance frequency and quality factor of the spectrophone under harsh volcanic conditions, characterized by rapidly changing temperature and relative humidity conditions in the measured [15, 30] °C and [60, 100] % ranges, respectively. Throughout three days of measurements, no significant variations in the spectrophone resonance properties were observed, indicating that it was not damaged or degraded by prolonged exposure to the volcanic environment. This has been further confirmed by the post-campaign validation procedure described in the Methods Section. Second, the laser driving current of the QEPAS sensor was tuned to a value corresponding to a spectral region without H_2S absorption lines, allowing the checking of the background noise level, an indicator of the integrity of the performance of the sensor. Figure 3 shows the QEPAS signal, expressed in ppm-unit, acquired at position P3 with the laser current set to I = 146.4 mA (red trace), targeting the H_2S absorption line at 3792.9 cm^{-1} (identical to the operating conditions used for the measurements presented in Figs. 1 and 2), and with the laser current switched to I = 143 mA (blue trace), corresponding to a wavelength where no H_2S absorption occurs.

When the laser current is shifted away from the H_2S absorption line, the QEPAS signal returns to a stable background level, exhibiting only noise fluctuations within the MDL, despite the continued presence of H_2S of the volcanic plume impinging on the QEPAS sensor. This control measurement exploits the intrinsic spectral selectivity of optical techniques, and represents a distinctive advantage over other sensing approaches such as EC sensors. It enables periodic, real-time verification of sensor reliability, effectively ruling out artefacts arising from interfering species, sensor drift or sensor poisoning that could otherwise compromise measurement accuracy.

Multi-signal correlation

The H_2S, CO_2 and H_2O signals, simultaneously acquired by the QEPAS sensor and the GasLab®Pro analyzer were analyzed to compare their temporal fluctuations and relative ratio. All three independent measurements displayed consistent temporal trends, as shown in Fig. 4.

These data were used to estimate the characteristic CO_2/H_2S ratio of the Pisciarelli fumarolic field.

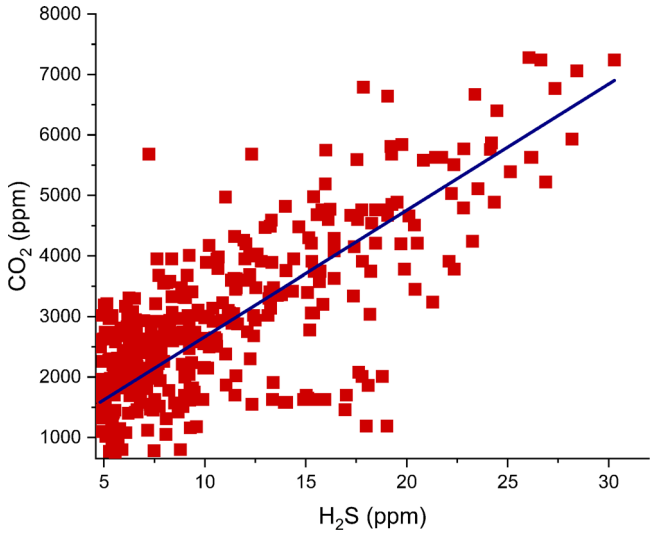

Fig. 5 | CO_2 concentration acquired with the NDIR sensor of the GasLab®Pro plotted as a function of the H_2S concentration measured with the QEPAS sensor. The blue solid line represents the best linear fit of the experimental data points.

Figure 5 shows the CO_2 concentration acquired with the GasLab®Pro sensor as a function of the H_2S concentration detected with the QEPAS sensor and their best linear fit.

The spread of the data is mainly ascribed to (i) the different precision of the two acquisition techniques and (ii) the different atmospheric dispersion behavior of CO_2 and H_2S. Indeed, the CO_2 persists in the area surrounding the plume with an elevated background compared to its typical atmospheric abundance, but with significant variability due to the combined effects of continuous CO_2 emission, atmospheric dilution, and plume dispersion. To reduce the effect of this short-term fluctuations (ii) and measurement noise (i), a moving average was applied to both CO_2 and H_2S time series before performing the linear regression. The regression was therefore performed on the averaged dataset, reducing the uncertainty on the slope. The intercept was fixed at 580 ppm, corresponding to the local background measured at the monitoring site when no H_2S was detected by the QEPAS sensor. This value is higher than the typical atmospheric concentration of ~420 ppm because the measurement site is located very close to the degassing area, where CO_2 is constantly released by the plume. The resulting fit yields a CO_2/H_2S slope of 208 ± 4 with a R-squared value of 0.92. This ratio is consistent with values reported in literature, obtained using electrochemical sensors for H_2S and NDIR analyzers for CO_2, which typically range between 150 and 350[24,34,35].

Discussion

This study demonstrated both the feasibility and the advantages of operating a QEPAS sensor in the harsh environment of an active volcanic area, offering fast, real-time, in-situ detection of trace components within a complex fumarolic gaseous matrix.

The high spectral selectivity of the QEPAS sensor allowed the detection of H_2S without interference from other gaseous species commonly present in fumarolic emissions, like H_2O, CO_2, CH_4, providing a strength point over the EC sensors. The signal stability is evidenced by the background noise acquired during field measurements (see Fig. 3), which is fully consistent with the laboratory performance of the sensor. The sensor's fast response time (1 s) proved to be a key point for accurately capturing the rapidly varying dynamics of H_2S emission and turbulence features of the plume (see Fig. 2). This capability prevents the loss of short-lived concentration peaks that slower sensors would fail to capture, thereby avoiding systematic underestimation of the actual H_2S concentration. A direct comparison with the INGV monitoring systems is not feasible, since two EC-MultiGAS sensors (not used for direct plume measurements) were located on opposite sides of the Pisciarelli vent and operated only 3 minutes per hour. The mean values recorded by the two fixed stations (V07 and MG3 in Fig. 1a) are 0.58 ppm and 0.16 ppm on May 28, 0.41 ppm and 0.45 ppm on May 29, with a maximum peak of 3.6 ppm. Despite the different positions and acquisition schedules, comparison with temporal trends observed in this study highlights the importance of using a fast-response sensor such as QEPAS. In this context, the capability to resolve rapid concentration fluctuations driven by plume turbulence and atmospheric mixing makes the combination of high selectivity, fast response time, and robustness in harsh environments more important than achieving sub-ppm sensitivity level.

H_2S data collected at the CFc using different sensors have been represented in Fig. 6a–b to highlight the differences in the estimated H_2S concentration and variability obtained with instruments characterized by different temporal resolutions. The data are presented using box-plot representation to allow comparison of concentration ranges, median values, and variability. The comparison was restricted to in-situ sensors detecting the H_2S content in air close to the Pisciarelli fumarole and include: (i) the data recorded by the INGV monitoring stations V07 and MG3 since February 2024 and August 2024, respectively, with an acquisition rate of one measurement per hour; (ii) the data acquired with the QEPAS sensor reported in this work, with a signal integration time of 1 s; (iii) the data published in[36], acquired using a ThermoFisher 450i instrument with a response time of approximately 1 min during a measurement campaign conducted at a distance of 85 m from the Pisciarelli vent. The long-term H_2S dataset based on a monthly passive sampling of fumarolic fluids was not included in this comparison, as it is not directly comparable with real-time in-situ measurements of plume composition, which is the focus of this work.

Figure 6a–b show the monthly box plots of the H_2S concentrations measured by the MultiGas-based monitoring stations V07 and MG3, respectively. The median values of the box plots indicate that EC sensors are able to capture variations in the average H_2S concentration over daily to monthly timescales, confirming their suitability for continuous monitoring and safety surveillance purposes. Figure 6c highlights the difference in detection capability and information content between the QEPAS and EC sensors. The box plots refer to the datasets acquired on 28 May 2025 and 29 May 2025, for both sensors. First, the median H_2S concentrations measured by the QEPAS sensor are higher than those recorded by the MultiGas stations, meaning that EC sensors tend to underestimate H_2S concentrations. Second, the whiskers (set to 1.5 times the interquartile range) and the outliers in the QEPAS box plots extend to significantly higher values compared to those of the MultiGas sensors. These features further stress the capability of QEPAS sensor to reconstruct short-lived high-concentration events that are lost with detection techniques with lower temporal resolution.

The cost of a QEPAS system is currently higher than that of a single MultiGAS unit, as the two techniques are designed for different purposes. MultiGAS instruments are well suited for distributed monitoring networks and long-term surveillance, whereas QEPAS sensors are more suitable for high–time-resolution measurements at selected locations. Therefore, the two techniques should be considered complementary rather than alternative. It is worth noting that a large fraction of the QEPAS system cost is due to the mid-infrared laser source. As mid-infrared laser technologies become more widely available, their cost is expected to decrease significantly, potentially reducing the overall cost of QEPAS-based sensors in the near future.

Finally, the H_2S concentrations measured in this work has been interpreted within the hydrothermal degassing framework of the CFc. Previous studies have shown that degassing at Pisciarelli and Solfatara is dominated by hydrothermal fluids, where H_2S represents the main reduced sulfur species, while SO_2 is largely scrubbed through interaction with the hydrothermal system. H_2S concentrations in air are therefore not only controlled by the source degassing rate, but also by plume dispersion, atmospheric dilution, and secondary oxidation processes, resulting in strong spatial and temporal variability. Atmospheric dispersion of H_2S emissions in the Solfatara–Pisciarelli area has been investigated using different

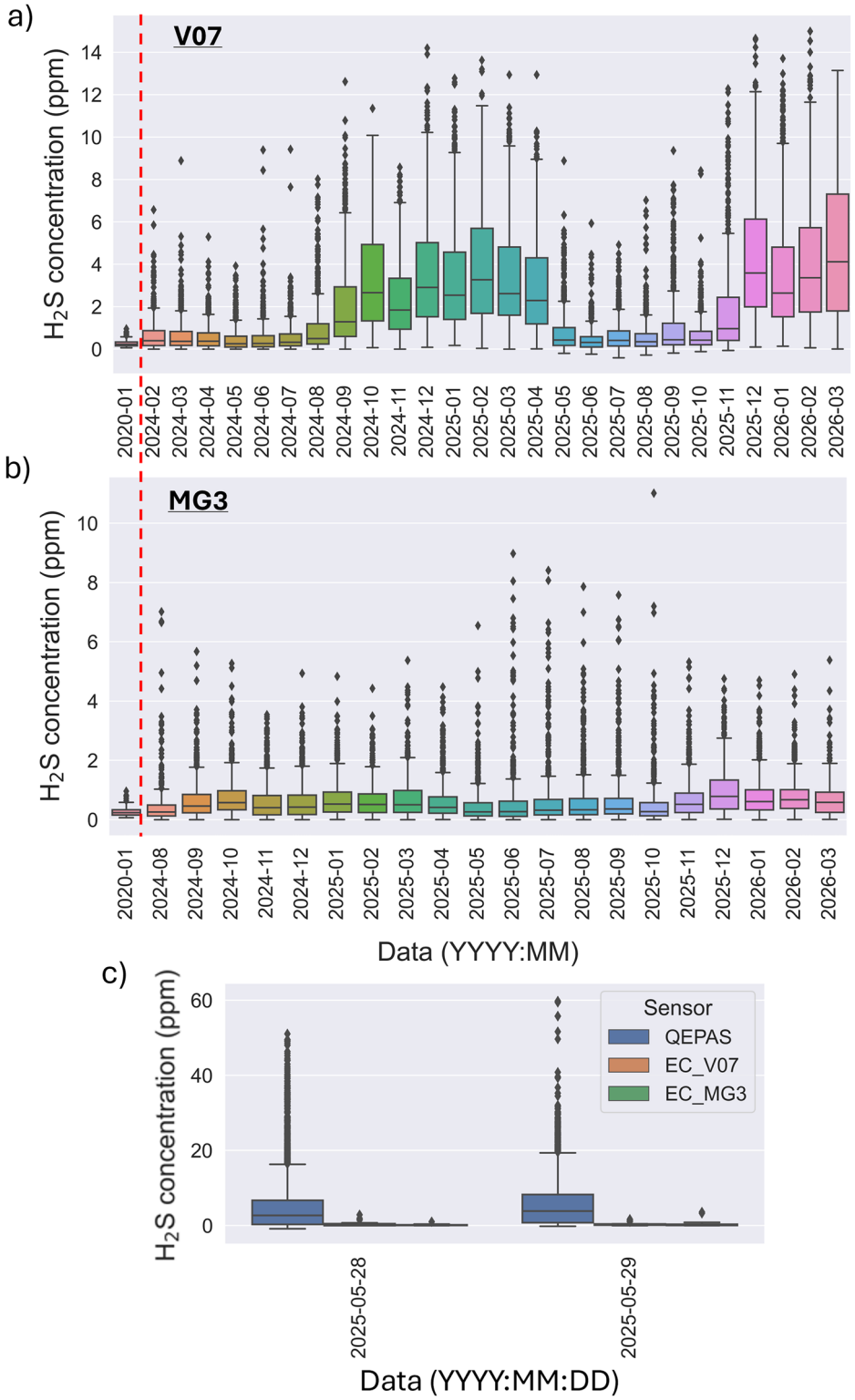

Fig. 6 | Box plot representation of the H_2S concentrations at the Phlegraean fields. H_2S monthly concentrations measured with the INGV EC-monitoring stations V07 (**a**) and MG3 (**b**) since 2024. The first box plot (corresponding to January 2020) represents the H_2S measurements reported in ref. 36, characterized by low H_2S concentrations since the sensor was at a distance of 85 m from the Pisciarelli source. **c** Box plots of the H_2S concentrations acquired on 28 May 2025 and 29 May 2025 with the QEPAS sensor (blue plot) and the INGV stations V07 (orange plot) and MG3 (green plot).

air-sampling methodologies, including passive/diffusive samplers (Radiello traps, diffusive tubes) and real-time analyzers (MultiGas, Thermo Fisher 450i). Passive samplers, which provide time-integrated measurements over extended exposure periods, reported localized H_2S concentrations in peripheral areas, but are not able to resolve short-term concentration fluctuations and may overestimate concentrations at low levels due to their cumulative sampling approach. To better frame the measurements performed in this work within the degassing context of the Campi Flegrei caldera, Table 2 summarizes the typical H_2S concentration ranges in air reported for different locations and measurement conditions in the Solfatara–Pisciarelli area, including background levels, peripheral areas and near-vent plume measurements.

High–time-resolution measurements of H_2S concentrations can provide information not only on gas abundance but also on plume dynamics, atmospheric mixing, and near-source dispersion processes. The combination of the H_2S QEPAS sensor with the GasLab®Pro CO_2/H_2O analyzer

operating at the same acquisition rate enabled direct comparison of their temporal patterns. The direct derivation of the CO_2/H_2S ratio provides higher accuracy and confidence in ratios produced, compared to the use of sensors with slow response time or showing different response times for different gases, which may underestimate peak concentrations and bias the estimation of gas ratios. Future integration of the sensing platform with a weather station equipped with an anemometer would further enable the correlation of CO_2 and H_2S concentration peaks with wind direction and enable direct estimation of their fluxes, without additional post-processing analysis[34].

Overall, the proposed system platform provides accurate concentration time series which can be deployed at active/dormant volcanoes sites for supporting daily control of the emissions and improving the quantification of volcanic gas dispersion for hazard assessment purposes. In particular, our results highlight the potential of the method to calibrate numerical dispersion models including the atmospheric effects on the H_2S, as shown for instance for CO_2 emissions at the Pisciarelli fumarolic field and Solfatara crater[37]. At the same time, the ability to resolve temporal variability and concentration gradients with increasing distance from the source would represent a significant advancement in H_2S emission monitoring, enabling the inclusion of chemical reactions in current gas dispersion models that do not explicitly account for them, as the Eulerian model DISGAS 2.6.0[38].

Table 2 | Typical H_2S concentration ranges in air measured in the Solfatara–Pisciarelli area under different measurement conditions and distances from the emission source

Measurement location	Measurement technique	H_2S (ppm)	Ref
Background	Direct Analyzer (Thermo Fisher 450i)	0.0001–0.01	43
Peripheral areas	Passive Samplers/ Analyzers	0.01–0.5 (spikes up to 4)	44
Near-vent plume	Direct Analyzer (MultiGas)	0.1–10 (spikes up to 20)	24
Near-vent plume	Passive samplers	Up to ~2.5	44
Near-vent plume	Direct Analyzer(QEPAS)	5–60	This work
Reference thresholds			
Thresholds type		**H_2S (ppm)**	
Odor threshold		~0.01	
Health limit short exposure		~5	
Dangerous		>20	

Similarly, providing a reliable dataset of sulfur content over time could substantially improve the development of geochemical models based on sulfur degassing (e.g., Sulfur_X[39]) and C-O-H-S equilibria[10]. In this framework, the proposed measurement approach is not only a technical improvement in gas sensing, but also a tool enabling more accurate interpretation of volcanic degassing processes.

While the field tests presented here focused on H_2S detection, the modular architecture of the QEPAS technique and the wavelength-independent detection scheme allow straightforward adaptation to other molecules of interest, like CH_4 or SO_2, by simply replacing the laser source. Additionally, advanced QEPAS configurations based on the use of two laser sources, in order to target the absorption lines of two different molecules, combined with a unique QTF detector have already been demonstrated for the simultaneous detection of two gas species or the isotopes of the methane[40], offering promising opportunities for future isotopic studies of H_2S and CH_4.

Methods

Quartz-enhanced photoacoustic spectroscopy sensor

A QEPAS sensor was developed for the detection of H_2S. QEPAS is based on the excitation of the vibrational energy states of the target gas through the absorption of modulated infrared laser light. The subsequent non-radiative relaxation of these excited states generates pressure waves which are detected by a quartz tuning fork (QTF). These pressure oscillations drive the mechanical vibrations of the QTF prongs, producing an electrical signal via the piezoelectricity of the quartz. The QEPAS system was assembled in a compact 19-inch rack (with size of 48.3 × 39.6 × 15.0 cm, weight of 10 kg and power consumption of 60 VA), housing the optical/sensing modules, electronic control units, and the gas-handling line. A schematic overview of the QEPAS sensor components is shown in Fig. 7.

The optical module of the sensor, consisting in the laser source, the focusing lens and the ADM, is mounted on a rigid support embedded in sound-absorbing foam. This structure has been properly designed to strongly improve the mechanical stability, preserve the optical alignment and minimize the influence of mechanical vibrations and ambient acoustic noise. The light source is an infrared diode laser (Nanoplus S/N: 2854/25-11) emitting at 2637.8 nm, mounted on a heat spreader equipped with heat pipes and a cooling fan to ensure efficient thermal dissipation. Laser current and temperature are controlled using an OEM laser driver and a miniature temperature controller (Thorlabs, model MTD1020T). The emitted beam is focused into the ADM by means of a 40 mm focusing lens. The ADM is a compact airtight gas cell having a volume of 7 cm^3, equipped with two windows for the laser light transmissions and with inlet/outlet connectors for the gas flow. It contains the spectrophone, consisting of a T-shaped QTF with prongs 9.4 mm long and 0.5 mm thick, spaced by 0.8 mm, and coupled

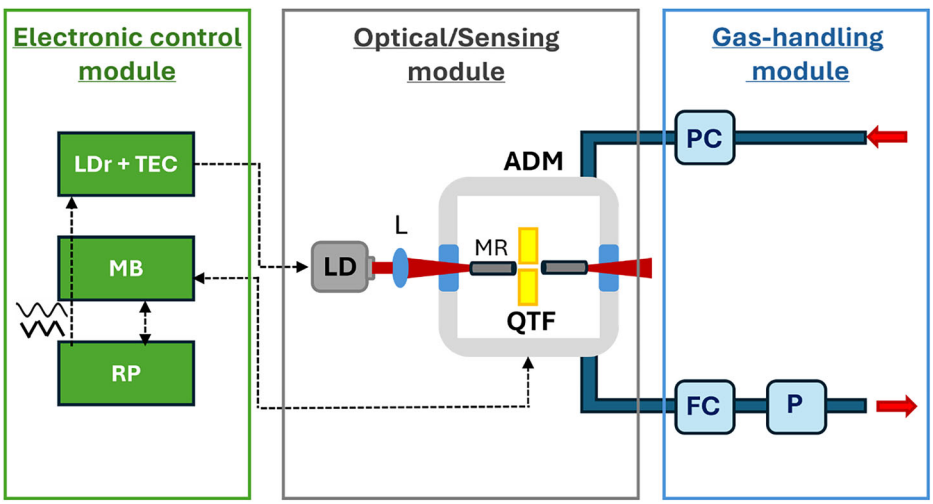

Fig. 7 | Schematic of the components of the QEPAS sensor. Green box: Electronic control module (LDr laser Driver, TEC Temperature Controller, MB Main Board, RP RedPitaya board). Gray box: Optical/ Sensing module (LD Diode Laser, L focusing lens, ADM Acoustic Detection Module, QTF Quartz Tuning Fork, MR Micro-Resonator tubes). Blue box: Gas-handling module (PC Pressure controller, FC Flow Controller, P Pump).

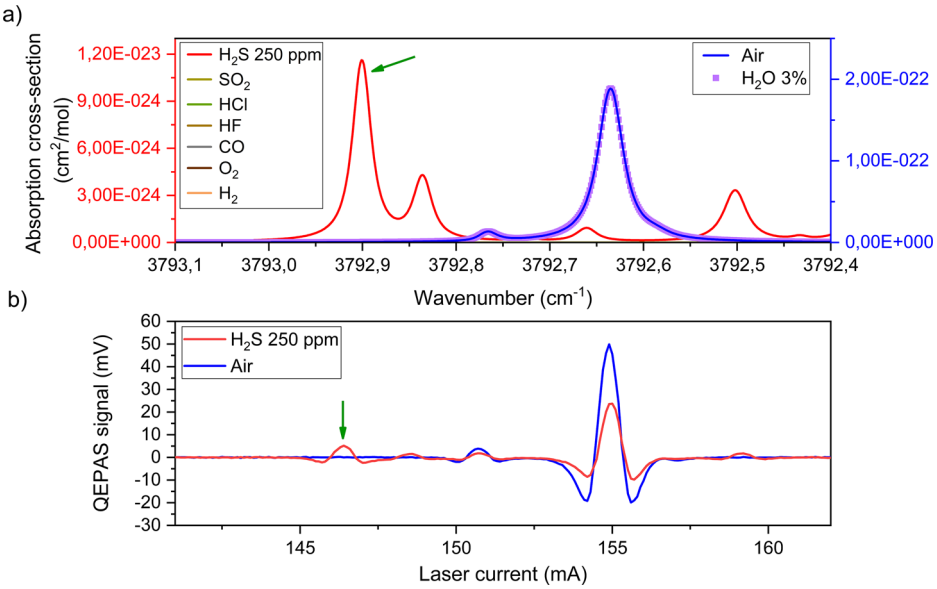

Fig. 8 | Selection of the H_2S absorption line. **a** Absorption spectrum of 250 ppm of H_2S (red trace), standard air (blue trace) and 3% of H_2O (violet squares) at 100 Torr simulated with HITRAN database; **b** QEPAS spectral scan of 250 ppm of H_2S in N_2 (red trace) and of laboratory air (blue trace) at 100 Torr. The green arrows indicate the selected H_2S absorption line and the corresponding QEPAS signal.

with a pair of resonator tubes having length of 12.4 mm and internal diameter of 1.51 mm, designed to boost the acoustic response. The laser light is focused through the tubes and between the prongs of the QTF at the antinode point of its fundamental vibrational mode. At 100 Torr, the fundamental frequency (f_0) and quality factor (Q) of the spectrophone are 12438.85 Hz and 26465, respectively. The narrow bandwidth of 0.45 Hz provides strong immunity to ambient acoustic noise. Gas temperature and humidity inside the ADM are monitored using an integrated hygrometer (IST, model HYT 221). The QEPAS sensor was operated in wavelength-modulation and second-harmonic (WM-2f) detection. A sinusoidal excitation at half of the QTF fundamental resonance frequency f_0 was applied to the laser current driver, while the QTF response signal was demodulated at f_0. The WM-2f detection technique provides background-free signals, avoiding the need for background subtraction or corrections on the acquired measurements.

The RedPitaya board (model STEMlAb 125-14) was used to generate the sinusoidal excitation applied to the laser current and to demodulate the acquired QTF signal, by means of a lock-in amplifier implemented on the field programmable gate array on the board. Spectral scans within the current dynamic range were obtained by superimposing a triangular ramp on the sinusoidal modulation. The gas-handling line, consisting of a diaphragm pump (THOMAS 1420 VR), a pressure controller (Alicat Scientific, model EPC- 15PSIA-P01/10 P) and a mass flow controller (Alicat Scientific BC-C1000-Air-232-NPT), maintains the ADM at an operating pressure of 100 Torr and a flow rate of 25 sccm. The selected flow rate ensures laminar flow conditions within the ADM, preventing turbulence and eddy formation that could affect the efficiency of the photoacoustic signal generation. Previous studies conducted with similar ADM geometry[41] demonstrated that flow rates below 50 sccm guarantee laminar flow conditions and stable QEPAS signal operation. The gas inlet of the QEPAS sensor system was equipped with an EU5 filter (compliant with the EN 779 standard) to prevent contamination of the ADM by dust and heavy particles. This filter provides a high filtration efficiency (>99%) for particles with diameters larger than 1 µm. The QEPAS sensor communicates with a personal computer via Ethernet, and all system components are controlled using a custom Python-based software, which also handles lock-in data reading and acquisition.

Electrical and optical characterization

Prior to the on-field measurement campaign, the QEPAS sensor was characterized under controlled laboratory conditions to assess its ultimate performances. The vibrational properties of the spectrophone were experimentally measured by electrically exciting the QTF, resulting in a resonance frequency of 12,438.85 Hz and a quality factor of 26,400 at 100 Torr. Then, the target H_2S absorption line was identified in order to ensure the highest selectivity considering all the potential interferences near the volcanic gas emission source. According to the analysis of monthly sampling conducted by the INGV at the Pisciarelli fumarolic field, the main potential interfering species are CH_4, CO_2, H_2O, Ar, N_2, H_2, He and CO. Other typical volcanic gases include SO_2, HCl and HF, which are common acid gases found in high and medium-temperature fumaroles (T >100 °C), and may therefore be absent in the CF caldera. The HITRAN database was used to simulate the absorption cross-section of a volcanic air matrix composed of H_2O: 3%; CO_2: 5%; CH_4: 10ppm; O_2: 20.9%; N_2O: 320 ppb; CO: 150 ppb; O_3: 30 ppb; N_2: 77.2%, in order to reproduce a mixture representative of the atmosphere near the CF caldera. Figure 8a shows the absorption cross-section of: (i) the volcanic air matrix (blue line) compared with a mixture of 3% H_2O in N_2 (violet squares), (ii) H_2S (red line), and (iii) pure SO_2, HCl, HF, CO, O_2, and H_2. Simulations of these latter species indicate that none of them exhibit absorption features within the emission wavelength range covered by the employed laser source. The spectral overlap between the volcanic air and the 3% H_2O:N_2 mixture suggests that the two features at 3792.63 cm^{-1} and 3792.77 cm^{-1} are attributable to the water vapor absorption. Figure 8b shows the QEPAS spectral scan acquired from a mixture of humified 250 ppm of H_2S:N_2 and from laboratory air. During these measurements, the laser operating temperature was set to 31 °C and the current was swept from 142 to 161 mA.

Among the various H_2S absorption features shown in Fig. 8a–b, the line at 3792.9 cm^{-1} with linestrength of 1.6×10^{-21} cm/mol is the most intense and is well isolated from the absorption features of water vapor located at 3792.63 cm^{-1} and at 3792.77 cm^{-1}. For this reason, it was selected as the target line for both the sensor calibration and the field measurements. All subsequent calibration steps and outdoor acquisition were conducted by setting the laser current to I = 146.4 mA, corresponding to the H_2S target absorption line (on-peak configuration), and by using a signal integration time of 1 s.

During the on-peak long-term measurements, wavelength stability was addressed using an approach based on an internal spectral reference. The nearby strong water vapor absorption line at 3792.63 cm^{-1} (see Fig. 8a), falling within the laser emission range, was exploited as reference to periodically verify possible wavelength drifts during the measurements. The current separation between the H_2O and H_2S absorption lines was calibrated in advance during laboratory characterization, allowing the operating current for H_2S detection to be adjusted accordingly when required. During

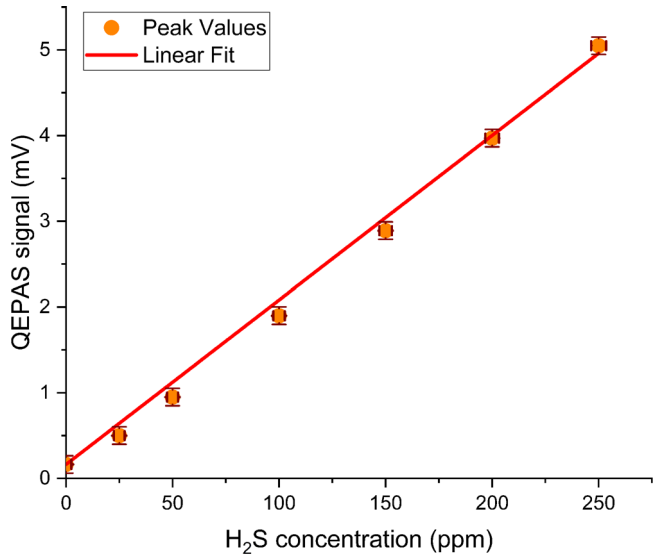

Fig. 9 | Mean peak values recorded for different H_2S concentration (orange circle symbols) and the corresponding best linear fit (red line) between QEPAS H_2S signal (mV) and H_2S concentration (ppm).

field measurements, the maximum observed current shift was 0.2 mA, which is sufficiently small not to significantly affect the targeting of the H_2S absorption line, thus ensuring stable and reliable sensor operation without the need for active wavelength locking.

The sensor was calibrated acquiring the on-peak QEPAS signal of the H_2S absorption line for different concentrations of H_2S in the [0, 250] ppm range. These mixtures were prepared by diluting a certified 250 ppm of H_2S:N_2 (extended uncertainty of 1%) with standard air using a gas mixer (MCQ Instrument Gas Blender 1003). The gas mixer flow accuracy is ~ 1%, as reported by the instrument datasheet, resulting in an accuracy on the H_2S concentration in the mixtures of ±2.5 ppm, starting from the certified gas cylinder concentration. The average QEPAS peak values recorded at each concentration are plotted as a function of the H_2S concentration in Fig. 9.

The calibration curve was obtained by fitting the experimental data points in Fig. 9 with a linear function setting the intercept at 0.163 mV, which corresponds to the noise level measured in the absence of H_2S in the ADM. The error bars on the QEPAS signal correspond to the 3σ noise of the sensor (0.102 mV), while the error bars on the concentrations were estimated starting from the extended uncertainty of the certified gas cylinder and the accuracy of the gas mixer, varying in the [2.5, 3.5] ppm range. The resulting sensitivity, given by the slope of the best-fit line, was 19.2 μV/ppm, with an uncertainty of ±0.5 μV/ppm. This corresponds to a relative error of about 2% in the H_2S concentration derived from the calibration curve, which is lower than the uncertainty associated with each measurement during the field campaign.

The obtained calibration curve was used in the plots shown in the Results section to convert the measured QEPAS signal into concentration of H_2S expressed in ppm.

Minimum detection limit estimation

The noise level of the sensor was measured by acquiring the QEPAS signal with the laser current set to I = 146.4 mA while flushing air through the ADM for several hours. This procedure was repeated on different days to assess the stability and repeatability of the measurement. The mean noise value was 0.163 mV, with a 1σ-value of 0.034 mV. Figure 10 shows the noise signal converted into H_2S concentration using the calibration curve reported in Fig. 9.

The 1σ-MDL was calculated as 1.6 ppm, representing the lowest gas concentration providing a signal-to-noise ratio of 1. Nevertheless, to ensure more reliable discrimination of the H_2S signal from background fluctuations, the 3σ noise level was used, resulting in a 3σ-MDL of 4.8 ppm.

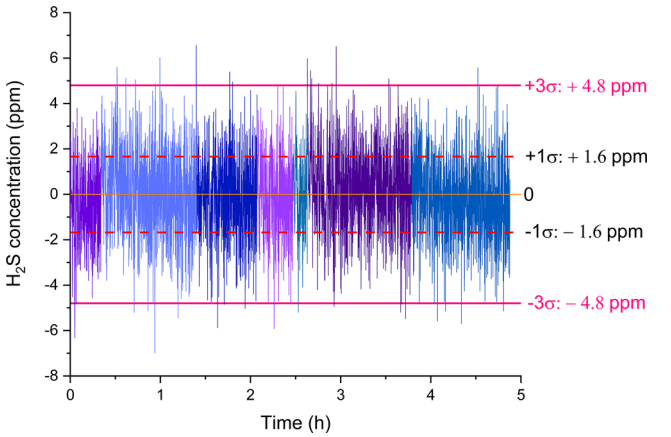

Fig. 10 | QEPAS noise signal converted in H2S concentration. The different colors represent the noise level acquired on 7 different days.

Table 3 | Comparison of the electrical characterization and calibration parameters before and after the measurements at the CF caldera

		Before CF	After CF	Discrepancy
Electrical characterization of the spectrophone	Resonance Frequency (Hz)	12438.85	12438.85	No difference
	Quality factor	26465	26353	~0.4%
Calibration of the QEPAS sensor	1σ-noise level	0.034	0.034	No difference
	Slope (μV/ppm)	19.2 ± 0.5	20.0 ± 0.5	~4%

Post measurement campaign validation

Both the electrical characterization of the QEPAS spectrophone and the calibration of the sensor were repeated in the laboratory after the measurement campaign at the CF, following the same procedures described in the two previous sub-sections. The results of both characterizations are summarized in Table 3.

The observed discrepancies were ≤ 4% for both the electrical and optical parameters, confirming that the sensor performance remained unaffected by operation in the caldera environment. This post-campaign verification of the spectrophone electrical properties as well as of the calibration of the QEPAS sensor itself confirmed that no degradation of the sensor components or no degradation of the performances occurred despite exposure to acidic volcanic gases. These results highlight the robustness of the QEPAS technique and demonstrate that no recalibration was required following field deployment.

GasLab Pro analyzer

The GasLab®Pro analyzer (model CM-1000) measures CO_2 concentration using the NDIR technology. The sensor has a CO_2 detection range of 0–20% with an uncertainty of ± 10 ppm. The device also includes an hygrometer to measure temperature and relative humidity (RH), with a temperature measurement range of 0–50 °C and an uncertainty of ±1 °C. The relative humidity measurement range is 0–100%, with an uncertainty of ±3% in the 20–80% RH range and ±5% outside this range, according to the manufacturer specifications.

Data availability

The datasets generated and analyzed during the current study are not publicly available since they consist of site-specific experimental

measurements requiring contextual interpretation but are available from the corresponding author on reasonable request.

Received: 19 January 2026; Accepted: 20 April 2026;
Published online: 29 April 2026

References

1. Sparks, R. S. J. Forecasting volcanic eruptions. *Earth Planet. Sci. Lett.* **210**, 1–15 (2003).
2. Chiodini, G. et al. Evidence of thermal-driven processes triggering the 2005–2014 unrest at Campi Flegrei caldera. *Earth Planet. Sci. Lett.* **414**, 58–67 (2015).
3. Caliro, S. et al. The origin of the fumaroles of La Solfatara (Campi Flegrei, South Italy). *Geochim. Cosmochim. Acta* **71**, 3040–3055 (2007).
4. Bevilacqua, A. et al. Accelerating upper crustal deformation and seismicity of Campi Flegrei caldera (Italy), during the 2000–2023 unrest. *Commun. Earth Environ.* **5**, 742 (2024).
5. Chiodini, G. et al. Clues on the origin of post-2000 earthquakes at Campi Flegrei caldera (Italy). *Sci. Rep.* **7**, 4472 (2017).
6. Giacomuzzi, G., Chiarabba, C., Bianco, F., De Gori, P. & Agostinetti, N. P. Tracking transient changes in the plumbing system at Campi Flegrei Caldera. *Earth Planet. Sci. Lett.* **637**, 118744 (2024).
7. Fischer, T. P. & Chiodini, G. Volcanic, Magmatic and Hydrothermal Gases. In *The Encyclopedia of Volcanoes* 779–797 (Elsevier, 2015). https://doi.org/10.1016/B978-0-12-385938-9.00045-6.
8. Giggenbach, W. F. Chemical composition of volcanic gases. In *Monitoring and Mitigation of Volcano Hazards* 221–256 (Springer Berlin Heidelberg, 1996).
9. Cynthia, W. et al. Carbon dioxide emissions from subaerial volcanic regions: two decades in review. In *Deep Carbon, Past to Present* (eds Orcutt, B. N., Daniel, I. & Dasgupta, R.) Vol. 1, 188–236 (Cambridge University Press, 2019).
10. Oppenheimer, C., Scaillet, B. & Martin, R. S. Sulfur degassing from volcanoes: source conditions, surveillance, plume chemistry and earth system impacts. *Rev. Mineral. Geochem.* **73**, 363–421 (2011).
11. Caliro, S. et al. Escalation of caldera unrest indicated by increasing emission of isotopically light sulfur. *Nat. Geosci.* **18**, 167–174 (2025).
12. Symonds, R. B. et al. Volcanic-gas studies: methods, results, and applications. In *Reviews in Mineralogy* vol. 30 (1994).
13. Horton, K. A. et al. Real-time measurement of volcanic SO2 emissions: validation of a new UV correlation spectrometer (FLYSPEC). *Bull. Volcanol.* **68**, 323–327 (2006).
14. Stoiber, R. E., Williams, S. N. & Huebert, B. Annual contribution of sulfur dioxide to the atmosphere by volcanoes. *J. Volcanol. Geotherm. Res.* **33**, 1–8 (1987).
15. Galle, B. et al. A miniaturised ultraviolet spectrometer for remote sensing of SO2 fluxes: a new tool for volcano surveillance. *J. Volcanol. Geotherm. Res.* **119**, 241–254 (2003).
16. Kantzas, E. P., McGonigle, A. J. S., Tamburello, G., Aiuppa, A. & Bryant, R. G. Protocols for UV camera volcanic SO2 measurements. *J. Volcanol. Geotherm. Res.* **194**, 55–60 (2010).
17. Oppenheimer, C. & Kyle, P. R. Probing the magma plumbing of Erebus volcano, Antarctica, by open-path FTIR spectroscopy of gas emissions. *J. Volcanol. Geotherm. Res.* **177**, 743–754 (2008).
18. Concas, F. et al. Low-Cost Outdoor Air Quality Monitoring and Sensor Calibration. *ACM Trans. Sens. Netw.* **17**, 1–44 (2021).
19. Chiodini, G. et al. Long-term variations of the Campi Flegrei, Italy, volcanic system as revealed by the monitoring of hydrothermal activity. *J. Geophys. Res.* **115**, 1–17 (2010).
20. Chiodini, G. et al. Hydrothermal pressure-temperature control on CO2 emissions and seismicity at Campi Flegrei (Italy). *J. Volcanol. Geotherm. Res.* **414**, 107245 (2021).
21. Buono, G. et al. New insights into the recent magma dynamics under Campi Flegrei Caldera (Italy) from petrological and geochemical evidence. *J. Geophys. Res. Solid Earth* **127**, 1–15 (2022).
22. Caliro, S., Chiodini, G. & Paonita, A. Geochemical evidences of magma dynamics at Campi Flegrei (Italy). *Geochim. Cosmochim. Acta* **132**, 1–15 (2014).
23. Pedone, M. et al. Volcanic CO2 flux measurement at Campi Flegrei by tunable diode laser absorption spectroscopy. *Bull. Volcanol.* **76**, 812 (2014).
24. Aiuppa, A. et al. First observations of the fumarolic gas output from a restless caldera: Implications for the current period of unrest (2005–2013) at Campi Flegrei. *Geochem. Geophys. Geosyst.* **14**, 4153–4169 (2013).
25. Edmonds, M., Herd, R. A., Galle, B. & Oppenheimer, C. M. Automated, high time-resolution measurements of SO2 flux at Soufrire Hills Volcano, Montserrat. *Bull. Volcanol.* **65**, 578–586 (2003).
26. Olafsdottir, S., Gardarsson, S. M. & Andradottir, H. O. Natural near field sinks of hydrogen sulfide from two geothermal power plants in Iceland. *Atmos. Environ.* **96**, 236–244 (2014).
27. Olafsdottir, S. & Gardarsson, S. M. Impacts of meteorological factors on hydrogen sulfide concentration downwind of geothermal power plants. *Atmos. Environ.* **77**, 185–192 (2013).
28. Thorsteinsson, T., Hackenbruch, J., Sveinbjörnsson, E. & Jóhannsson, T. Statistical assessment and modeling of the effects of weather conditions on H2S plume dispersal from Icelandic geothermal power plants. *Geothermics* **45**, 31–40 (2013).
29. Aiuppa, A. et al. The tropospheric processing of acidic gases and hydrogen sulphide in volcanic gas plumes as inferred from field and model investigations. *Atmos. Chem. Phys.* **7**, 1441–1450 (2007).
30. Kristmannsdóttir, H., Sigurgeirsson, M., Ármannsson, H., Hjartarson, H. & Ólafsson, M. Sulfur gas emissions from geothermal power plants in Iceland. *Geothermics* **29**, 525–538 (2000).
31. De Palo, R. et al. Quartz-enhanced photoacoustic sensors for detection of eight air pollutants. *Adv. Photonics Res.* **4**, 1–11 (2023).
32. Olivieri, M., Zifarelli, A., Sampaolo, A., Spagnolo, V. & Patimisco, P. Time-resolved analysis of carbon monoxide emissions from vehicles using a quartz-enhanced photoacoustic sensor. *Opt. Laser Technol.* **192**, 113879 (2025).
33. Khan, M. A. H., Rao, M. V. & Li, Q. Recent advances in electrochemical sensors for detecting toxic gases: NO2, SO2 and H2. *S. Sens.* **19**, 905 (2019).
34. Tamburello, G. et al. Escalating CO2 degassing at the Pisciarelli fumarolic system, and implications for the ongoing Campi Flegrei unrest. *J. Volcanol. Geotherm. Res.* **384**, 151–157 (2019).
35. Silvestri, M. et al. MultiGAS Detection from Airborne Platforms on Italian Volcanic and Geothermal Areas. *Remote Sens. (Basel).* **15**, 2390 (2023).
36. Biagi, R., Tassi, F., Caliro, S., Capecchiacci, F. & Venturi, S. Impact on air quality of carbon and sulfur volatile compounds emitted from hydrothermal discharges: The case study of Pisciarelli (Campi Flegrei, South Italy). *Chemosphere* **297**, 134166 (2022).
37. Massaro, S. et al. Turbulent diffusion and volcanic gas dispersion in the atmospheric surface layer: insights from La Solfatara, Campi Flegrei, Italy. *Earth, Planets Space* **77**, 143 (2025).
38. Massaro, S. et al. Quantification of volcanic degassing and analysis of uncertainties using numerical modeling: the case of Stephanos crater (Nisyros Island, Greece). *Bull. Volcanol.* **86**, 95 (2024).
39. Ding, S., Plank, T., Wallace, P. J. & Rasmussen, D. J. Sulfur_X: a model of sulfur degassing during magma ascent. *Geochem. Geophys. Geosyst.* **24**, 1–30 (2023).
40. Olivieri, M. et al. Simultaneous detection of $^{12}CH_4$, $^{13}CH_4$, and related isotope ratio exploiting a frequency-multiplexed mid-infrared quartz-enhanced photoacoustic sensor. *ACS Sens.* https://doi.org/10.1021/acssensors.5c02871 (2025).
41. Zifarelli, A. et al. Effect of gas turbulence in quartz-enhanced photoacoustic spectroscopy: a comprehensive flow field analysis. *Photoacoustics* **38**, 100625 (2024).
42. Shinohara, H. A new technique to estimate volcanic gas composition: plume measurements with a portable multi-sensor system. *J. Volcanol. Geotherm. Res.* **143**, 319–333 (2005).

43. Cabassi, J. et al. A new approach for the measurement of gaseous elemental mercury (GEM) and H 2 S in air from anthropogenic and natural sources: Examples from Mt. Amiata (Siena, Central Italy) and Solfatara Crater (Campi Flegrei, Southern Italy). *J. Geochem. Explor.* **175**, 48–58 (2017).
44. Venturi, S. et al. Hydrogen sulfide measurements in air by passive/diffusive samplers and high-frequency analyzer: a critical comparison. *Appl. Geochem.* **72**, 51–58 (2016).
45. Google. Google Earth. https://earth.google.com/web/ (2026).

Acknowledgements

The authors acknowledge financial support from the MUR project -Dipartimenti di Eccellenza 2023-2027-"Quantum Sensing and Modeling for OneHealth" (QuaSiModO) and MUR project "Sviluppo di sensori ottici per Monitoraggio in Aree Geografiche a rischio vulcanico di H2S e SO2 con sistemi Mobili, compatti e ad Alta sensibilità" (MAGMA) PE00000005 – CUP: H93C22000610002.

Author contributions

A.E. and P.P. co-wrote the paper; A.E., P.P., and M.O. conceived the experiment; A.E., P.P., and M.O. carried out the experiment, together with F.R.; A.E. carried out the data analysis; A.E. prepared figures; S.M., R.S., C.S., C.A., D.P., and R.F. worked on the methodology and conceptualization; P.P., V.S., and A.S. acquired the funding; all authors participated in the discussion of the results; all authors reviewed the manuscript.

Competing interests

The authors declare no competing interests.

Additional information

Correspondence and requests for materials should be addressed to Pietro Patimisco.

Reprints and permissions information is available at http://www.nature.com/reprints

Publisher's note Springer Nature remains neutral with regard to jurisdictional claims in published maps and institutional affiliations.

Open Access This article is licensed under a Creative Commons Attribution-NonCommercial-NoDerivatives 4.0 International License, which permits any non-commercial use, sharing, distribution and reproduction in any medium or format, as long as you give appropriate credit to the original author(s) and the source, provide a link to the Creative Commons licence, and indicate if you modified the licensed material. You do not have permission under this licence to share adapted material derived from this article or parts of it. The images or other third party material in this article are included in the article's Creative Commons licence, unless indicated otherwise in a credit line to the material. If material is not included in the article's Creative Commons licence and your intended use is not permitted by statutory regulation or exceeds the permitted use, you will need to obtain permission directly from the copyright holder. To view a copy of this licence, visit http://creativecommons.org/licenses/by-nc-nd/4.0/.

© The Author(s) 2026